coatings

MDPI

Article

Investigation of the Microhardness, Morphology, and Wear Resistance of A7075 Subjected to Machine Hammer Peening

Yu Liu [1,2], Yefu Wang [1], Lu Yu [2], Ying Yang [2], Ning Nie [3], Xingxing Wang [2,*] and Yifu Shen [1,*]

[1] College of Materials Science and Technology, Nanjing University of Aeronautics and Astronautics, Nanjing 211106, China; liuyu_me@ntu.edu.cn (Y.L.); yfwang_nuaa@163.com (Y.W.)
[2] School of Mechanical Engineering, Nantong University, Nantong 226019, China; 2310110003@stmail.ntu.edu.cn (L.Y.); 2010110242@stmail.ntu.edu.cn (Y.Y.)
[3] School of MMMB, University of Wollongong, Wollongong, NSW 2522, Australia; ningnie@uow.edu.au
* Correspondence: wangxx@ntu.edu.cn (X.W.); shenyifu0501@gmail.com (Y.S.)

Abstract: In industrial production, 7075 aluminum alloy (A7075) is prized for its strength and light weight. However, heat treatment can reduce its hardness and wear resistance. Therefore, proper surface treatments are often necessary to optimize its mechanical properties. In this work, a hammering tool attached to a robotic arm was employed to impact the surface of A7075 using different impact energies, and the surface hardness, morphology, roughness, and frictional characteristics of samples subjected to machine hammer peening (MHP) treatment were analyzed to explore the strengthening mechanism of MHP. The results indicate that the hardness increased to a maximum value of 235 HV with rising impact energy, whereas the depth of influence (2 mm) was almost unaffected by the impact energy. Microstructural analysis revealed significant grain refinement, especially at 2.7 J. The surface roughness increased significantly to about 7.2 μm, then dropped to around 3.7 μm when the impact energy increased to 2.7 J. Finally, the roughness decreased to ~6.8 μm. In addition, the samples that were strengthened by MHP demonstrated low friction coefficients (about 0.27) and wear volume (minimum value of $7.67/10^{-4}$ mm^3), implying that MHP can effectively improve the wear resistance of A7075. Observation by SEM revealed that the corresponding wear mechanism is mainly attributable to mild oxidative wear and three-body wear.

Keywords: 7075 Al alloy; machine hammer peening; microhardness; surface morphology; wear resistance

Citation: Liu, Y.; Wang, Y.; Yu, L.; Yang, Y.; Nie, N.; Wang, X.; Shen, Y. Investigation of the Microhardness, Morphology, and Wear Resistance of A7075 Subjected to Machine Hammer Peening. *Coatings* **2024**, *14*, 1481. https://doi.org/10.3390/coatings14121481

Academic Editor: Michał Kulka

Received: 26 September 2024
Revised: 16 November 2024
Accepted: 21 November 2024
Published: 22 November 2024

1. Introduction

Due to its high strength, low density, and good processability, 7xxx series aluminum (Al) alloys are widely used in aerospace, automotive industry, electronics, and so on. However, the susceptibility of the alloys to localized corrosion [1] significantly constrains their broader application.

Heat treatment is commonly used to improve the corrosion resistance of 7xxx series Al alloys. Previously, it was found that the discontinuously distributed precipitates at grain boundaries, which are formed during the aging process, could enhance the corrosion resistance of Al alloy [2]. The size and distribution of these precipitates are crucial to corrosion resistance [3]. However, heat treatment often leads to a deterioration in the mechanical properties of these alloys.

Alloying is one of the methods employed to enhance the mechanical properties of Al alloys. Unfortunately, the subsequent improvement in mechanical properties often comes at the expense of reduced corrosion resistance. In recent decades, various strengthening technologies have been studied by researchers to address the challenge of balancing mechanical properties and corrosion resistance in these alloys [4–6]. Among these, the development of gradient materials has emerged as a promising approach, offering

improvement in strength without altering the elemental composition of alloys. Gradient materials exhibit a gradual change in microstructure and mechanical properties from the surface to the interior. Typically, the outer surface might be designed to have fine grains and high hardness, while the interior retains coarse grains and good ductility, thereby providing overall better mechanical performance without sacrificing durability.

Surface treatment techniques, such as shot peening [7], cavitation water jet peening [8], laser shock peening [9], and sliding friction treatment [10], can induce severe plastic deformation on material surfaces to form a gradient structure. This process results in high dislocation density [11], significant residual compressive stress [12], and refined surface structures [13], effectively enhancing the hardness, wear resistance, and fatigue properties of these components. Shot peening is a traditional and effective surface treatment method. However, the use of solid balls made of steel, ceramics, or glass beads can introduce contamination to material surfaces [14]. Li et al. revealed that the contaminants from shot peening, such as Fe and Cr from stainless steel shot or Al from aluminum shot, can lead to the formation of an oxide layer on the material's surface, which can degrade the corrosion resistance of the treated material [15]. Cavitation water jet peening and laser shock peening can achieve surface nanocrystallization with minimal or no contamination, as their shot media are water and lasers, respectively. However, the limited impact depth of cavitation water jet peening [16] and the complex operation and high costs associated with laser shock peening have become significant barriers to their widespread application [17].

Machine hammer peening (MHP) is an advanced surface treatment process used to improve the hardness, wear resistance, and fatigue performance of materials. It involves the use of a hammering tool, typically attached to a CNC machine or robotic arm, which repeatedly impacts the surface of the material. This process substantially refines the surface structure [18], introduces beneficial compressive stresses [19], and can significantly enhance surface quality without introducing any contamination [20,21]. Jin et al. [22] demonstrated that the precisely controlled impacts of the MHP punching head can significantly smooth the impacted surface. In comparison, studies have reported that the surface roughness tended to increase after SP treatment [23] and LSP treatment [24]. Meanwhile, the MHP process generates a sub-surface residual stress field with an effective depth exceeding 1 mm and a maximum compressive stress reaching about 1.5 GPa, along with an approximate improvement in microhardness of 49%. In contrast, SP treatment could produce a 75 μm-deep residual stress field [25], while the LSP process could introduce residual stress to a depth of 400 μm [24], indicating that MHP technology is capable of producing a significantly deeper residual stress field.

Recently, the MHP technique has shown great promise as a post-processing method for improving the surface integrity and mechanical properties of workpieces produced by wire-based laser metal deposition. Dadgar et al. [26] reported that MHP substantially improved surface properties by reducing roughness and increasing hardness, indicating its promising application in the field of additive manufacturing.

Currently, most research on the MHP technique focuses on microhardness, roughness, and residual stress. Few studies have been carried out on the wear resistance of materials subjected to MHP. Bleicher and his colleagues [27] proposed that wear resistance can be enhanced by MHP technology and found that after MHP treatment, coated tool steel demonstrated a significant reduction in wear during tribometer tests. Similarly, Ripoll et al. [28] investigated the feasibility of using machine hammer peening to embed tungsten carbide particles of various sizes onto engineering substrate materials. The result demonstrated that this technique effectively enhances wear resistance, offering significant potential for applications on tribologically loaded surfaces. However, these studies have not revealed the tribological behavior and wear mechanism of MHP-treated samples.

The 7075 Al alloy (A7075) used herein is one of the most widely used alloys in the 7xxx series. In the present work, A7075 was selected to study the influence of MHP impact energies on the material's wear resistance. Microhardness, surface morphology, and tribological behavior were systematically analyzed using confocal microscopy, scanning

electron microscopy (SEM), and electron backscatter diffraction (EBSD) to reveal the underlying friction mechanisms.

2. Experimental Materials and Procedures

2.1. Materials and MHP Process

The material selected for this experiment was an A7075 sheet; its chemical composition is detailed in Table 1. The data source is the manufacturer's material certificate. Initially, the sample sheet was cut to dimensions of 30 × 30 × 10 mm^3. The specimens were then heat-treated at 520 °C for 3 h, followed by air cooling.

Subsequently, an electric impact hammer system with a head 5 mm in diameter was used for the hammering experiment, as illustrated in Figure 1. To ensure uniform treatment of the sample surface, hammering was conducted for 10 min at impact energies of 0, 1.7, 2.7, and 3.5 J, respectively. The specimens were accordingly designated as unMHP, MHP1.7, MHP2.7, and MHP3.5.

Table 1. Chemical composition of A7075 in wt.%.

Elements (wt.%)	Si	Fe	Cu	Mn	Mg	Cr	Zn	Ti	Al
A7075	0.40	0.50	1.20	0.30	2.10	0.18	5.10	0.20	Bal.

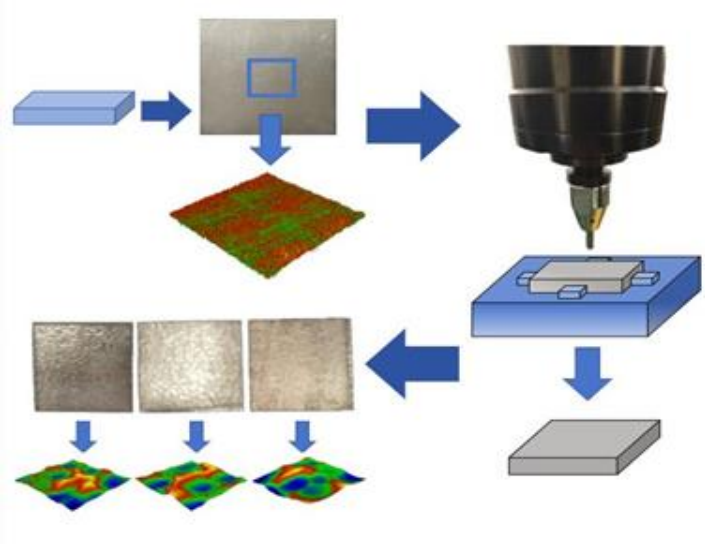

Figure 1. Machine hammer peening flow chart.

2.2. Microhardness

To measure the microhardness of the A7075 sheet, samples were cut to dimensions of 10 × 3 × 10 mm^3. An ultrasonic cleaner with anhydrous ethanol was then used to remove surface contaminants and residual cutting debris. A digital microhardness tester (HV-1000, Shidai Yiqi, Beijing, China) was then employed to apply a load of 200 g for 15 s on the sample surface. As shown in Figure 2, the transverse plane (i.e., the RD-ND plane) of the sample was used as the measurement plane. The first test point was located 100 μm from the sample's edge along the normal direction, with subsequent test points spaced 200 μm apart in the same direction. Along the rolling direction, the spacing between test points was set at 300 μm to prevent interference from the plastic deformation of adjacent points. To minimize errors from surface irregularities due to hammering, each sample underwent three sets of measurements, with the average value being recorded and calculated.

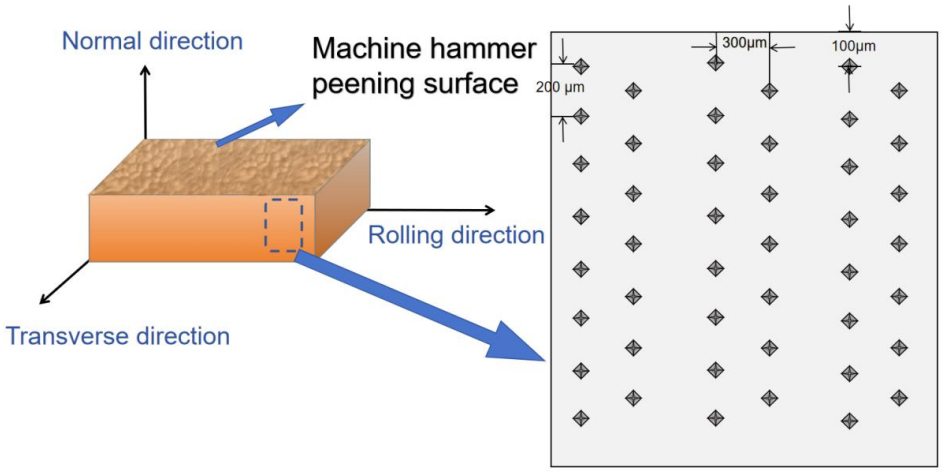

Figure 2. Microhardness test diagram.

2.3. Surface Topography

In order to investigate the effect of MHP treatment on the surface morphology and roughness of A7075, high-resolution confocal microscopy (μsurf mobile, NanoFocus, Germany) was used to observe and measure the surface characteristics of the sample. Two groups of samples were observed: the untreated (raw) sample and the samples subjected to MHP treatment at varying energy levels. The three-dimensional morphology, roughness value, and surface height difference of the samples before and after treatment were compared, and the changes in the different hammer parameters were analyzed. Additionally, a meticulous examination of the coating's surface morphology and elemental composition was carried out using a field-emission SEM (ZEISS Gemini SEM 300, ZEISS, Oberkochen, Germany), which was equipped with an EBSD detector (Oxford Instruments, Abingdon, UK) and an energy-dispersive X-ray spectrometer (EDS). The EBSD scans were undertaken at a voltage of 20 kV and at a working distance of 15 mm, with a scan step size of 0.4 μm.

2.4. Friction and Wear Testing

In this study, a multifunctional friction tester (MFT-5000, RTEC Instruments Inc., San Jose, CA, USA) was used to conduct friction and wear tests on the samples. The experiment employed a pin-on-flat reciprocating sliding contact method, with a pin composed of SiC. Before testing, the samples were cleaned, dried, and then secured in the friction tester's fixture. The reciprocating friction tests were conducted on A7075 at room temperature, with a frequency of 1 Hz and a load of 50 N for 10 min. Each test was repeated three times to minimize measurement errors. Subsequently, a high-resolution confocal microscope was used to observe the three-dimensional morphology.

3. Results and Discussion

3.1. The Distribution of Microhardness

As a surface treatment technology, MHP can lead to considerable changes in mechanical properties along the thickness direction of materials. The microhardness distributions of unMHP and MHP samples are illustrated in Figure 3. Undoubtedly, a substantial increase in hardness can be observed in the surface and sub-surface layers after MHP treatment, indicating that MHP is an effective method for surface strengthening. Specifically, the surface microhardness ascends with the increase in impact energy, and the maximum value of approximately 232 HV was achieved at an impact energy of 3.5 J, representing an increase of around 21%. However, the microhardness values of all MHP-treated specimens decreased with increasing depth, ultimately leveling off at about 193 HV, which corresponds to the hardness level of the untreated samples.

Generally speaking, the influence depth of peening techniques is linked to the impact energy [6,7,29]. Interestingly, all maximum influence depths stabilize at a depth of around 2 mm. Similar phenomena have been observed in other studies [16,30] involving the same materials. It is well known that the factors affecting hardness are associated with the densities of dislocation and the grain boundary under the same materials and working conditions [31,32]. As the impact energy increases, the dislocation density reaches a maximum value, due to the dynamic balance between dislocation formation and annihilation at a certain depth.

Compared to other peening techniques, MHP exhibits superior surface-strengthening capabilities. Zhang et al. [16] reported that the maximum influence depth of A7075 treated with cavitation water jet peening is around 0.6 mm, significantly less than the 2 mm depth achieved in our work. Similarly, Abeens et al. [7] compared the strengthening effect of A7075 subjected to different surface modification processes, including shot peening, severe surface mechanical treatment, and laser shock peening, and found that the maximal value of influence depth reached only 0.6 mm. The comparative results highlight that MHP has a distinct advantage over its counterparts and has a wide application perspective.

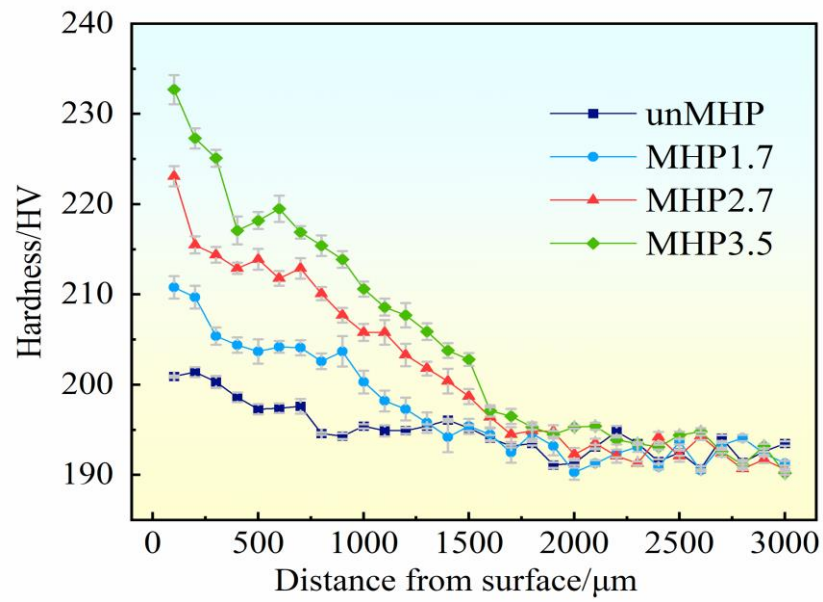

Figure 3. Microhardness distribution of the samples before and after MHP treatment.

3.2. Microstructure Evolution

The inverse pole figure color coding of the orientation maps in Figure 4 shows the microstructure evolution of MHP-treated samples. High-angle grain boundaries (HAGBs) ($\theta \geq 10°$) are indicated by black lines, while low-angle grain boundaries (LAGBs) ($2° \leq \theta < 10°$) are shown as grey lines in the figure. The color of each grain in the EBSD map represents the orientation of the RD of the sample's coordinate system relative to a specific crystallographic direction.

MHP treatment clearly induces substantial changes in microstructure. Specifically, the average grain size (using the equivalent circular diameter) is approximately 26.8 μm in the unMHP sample. In contrast, severe grain fragmentation can be observed after MHP treatment. The significant increase in the number of grains in the structure and substructure results in a reduced grain size. As demonstrated in Figure 5a, the mean grain size drops dramatically to about 14.0 μm in the MHP1.7 sample. With further increases in the impact energy to 2.7 J and 3.5 J, the average grain sizes drop and stabilize at around 10.5 and 10.9 μm, respectively.

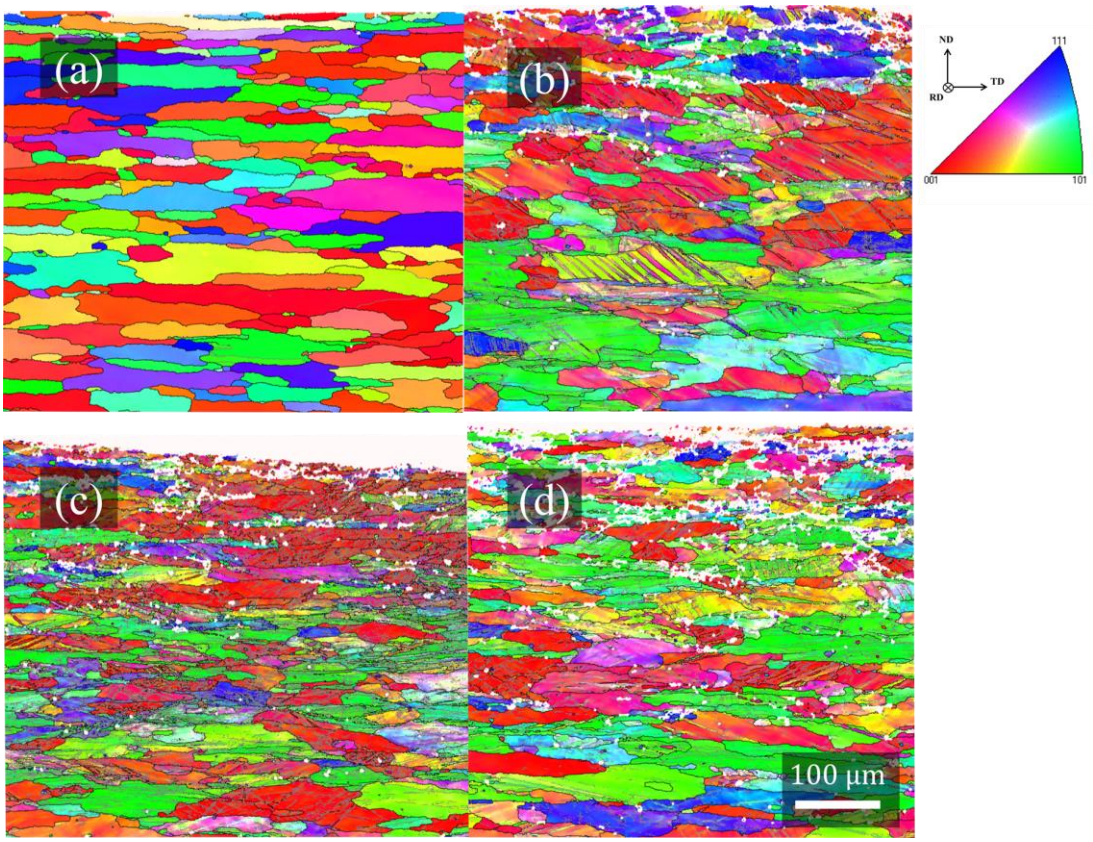

Figure 4. Microstructural characteristics of A7075: EBSD IPF maps of (**a**) unMHP, (**b**) MHP1.7, (**c**) MHP2.7, and (**d**) MHP3.5.

As a surface treatment technology, the most pronounced grain refinement occurs at the surface and sub-surface layers, and the refinement effect diminishes progressively with increasing depth. Closer inspection reveals that numerous small grains, ranging in size from 1 to 3 μm, are present in the surface and sub-surface regions. However, such refined grains are only detected within a depth of about 20 μm. Admittedly, neither nano-grained nor ultrafine-grained structures were observed in the current study. To evaluate the grain size distribution as a function of depth, the average grain sizes within a depth of 100 μm (Top100) are depicted in Figure 5a. Compared to the full-area grain size in the same sample, the moderate decrease in grain size within the Top100 region indicates that MHP technology cannot lead to severe grain refinement in 7075 Al alloy.

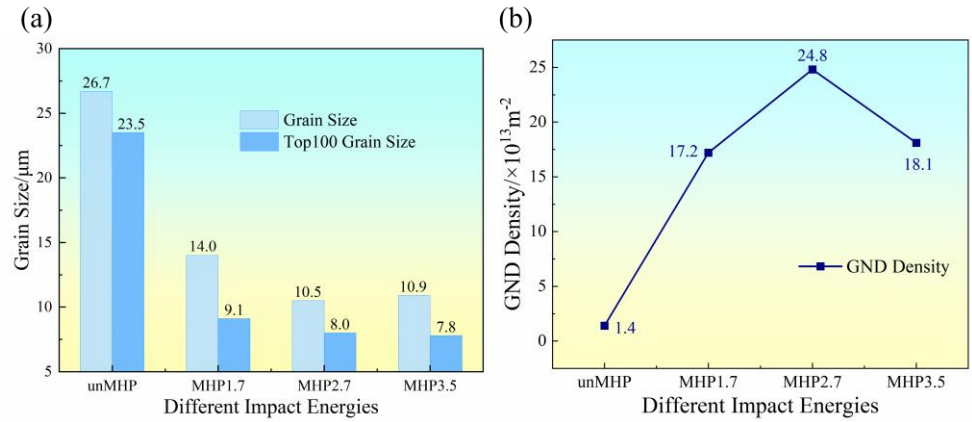

Figure 5. (**a**) The average grain size and (**b**) the GND density of different MHP samples.

However, the absence of nano-grained or ultrafine-grained structures does not indicate that MHP is an ineffective surface treatment method. MHP can significantly enhance the geometrically necessary dislocation (GND) density. As shown in Figure 5b, the GND density in the unMHP sample is about 1.40×10^{13} m^{-2}, which increases sharply to 17.1×10^{13}, 24.8×10^{13}, and 18.1×10^{13} m^{-2} for MHP1.7, MHP2.7, and MHP3.5, respectively. The distribution of GND is illustrated in Figure 6. It is noteworthy that the distribution of GND is uneven, with GND concentrated primarily within a depth of 400 μm. The depth corresponds to the region with the highest hardness values, implying that the sub-structure plays a significant role in the strengthening of MHP-treated 7075 Al alloy.

According to the data, the smallest grain size and highest GND density are found in the MHP2.7 sample. This refined grain structure can enhance hardness and wear resistance, demonstrating that the energy level is a potential parameter for MHP surface strengthening.

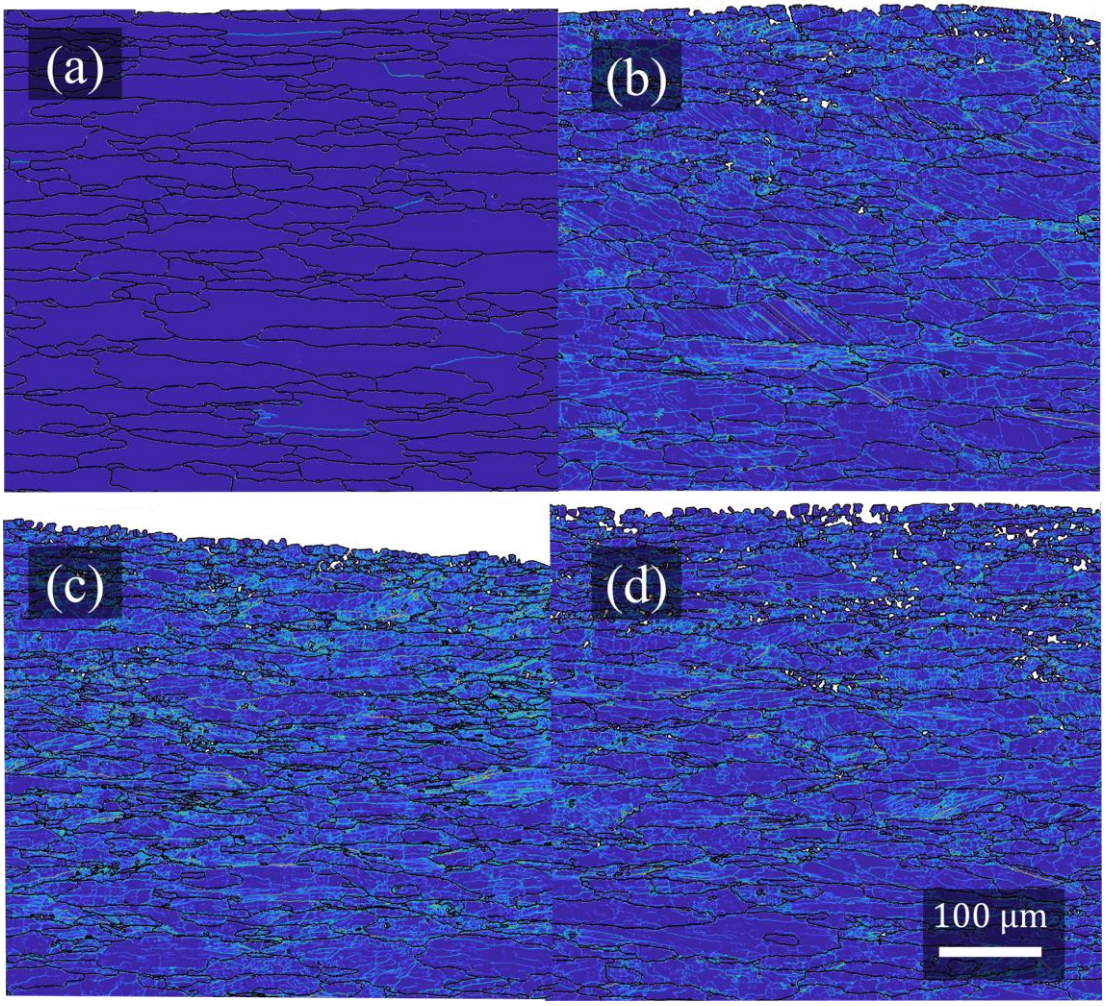

Figure 6. GND distribution maps of (**a**) unMHP, (**b**) MHP1.7, (**c**) MHP2.7, and (**d**) MHP3.5.

Changes in GND density are frequently accompanied by alterations in grain boundaries. Specifically, low-angle grain boundaries (LAGBs) (red lines) are barely observable in the unMHP sample due to annealing, as shown in Figure 7. With increasing energy, the number and the fraction of LAGBs increase to a high level. As demonstrated in Figure 8a, the proportion of LAGBs ascends from 2.59% in the unMHP sample to over 75% in the MHP-treated samples. Despite the decrease in the fraction of high-angle grain boundaries (HAGBs) (black lines), their absolute number increases simultaneously. Figure 8b illustrates the evolution of HAGB length. It should be noted that the grain boundary length

measured in EBSD is purely two-dimensional information because it represents the boundary's projection onto the sample surface. However, the magnitude of the increase in HAGB length effectively reflects the overall increase trend in HAGB evolution. Therefore, the concept of the HAGB length ratio, which is defined as the ratio of the HAGB length of the MPH-treated sample to that of the unMPH sample, is employed in this study. The increasing trend in HAGB length indicates effective grain fragmentation and refinement during MHP treatment.

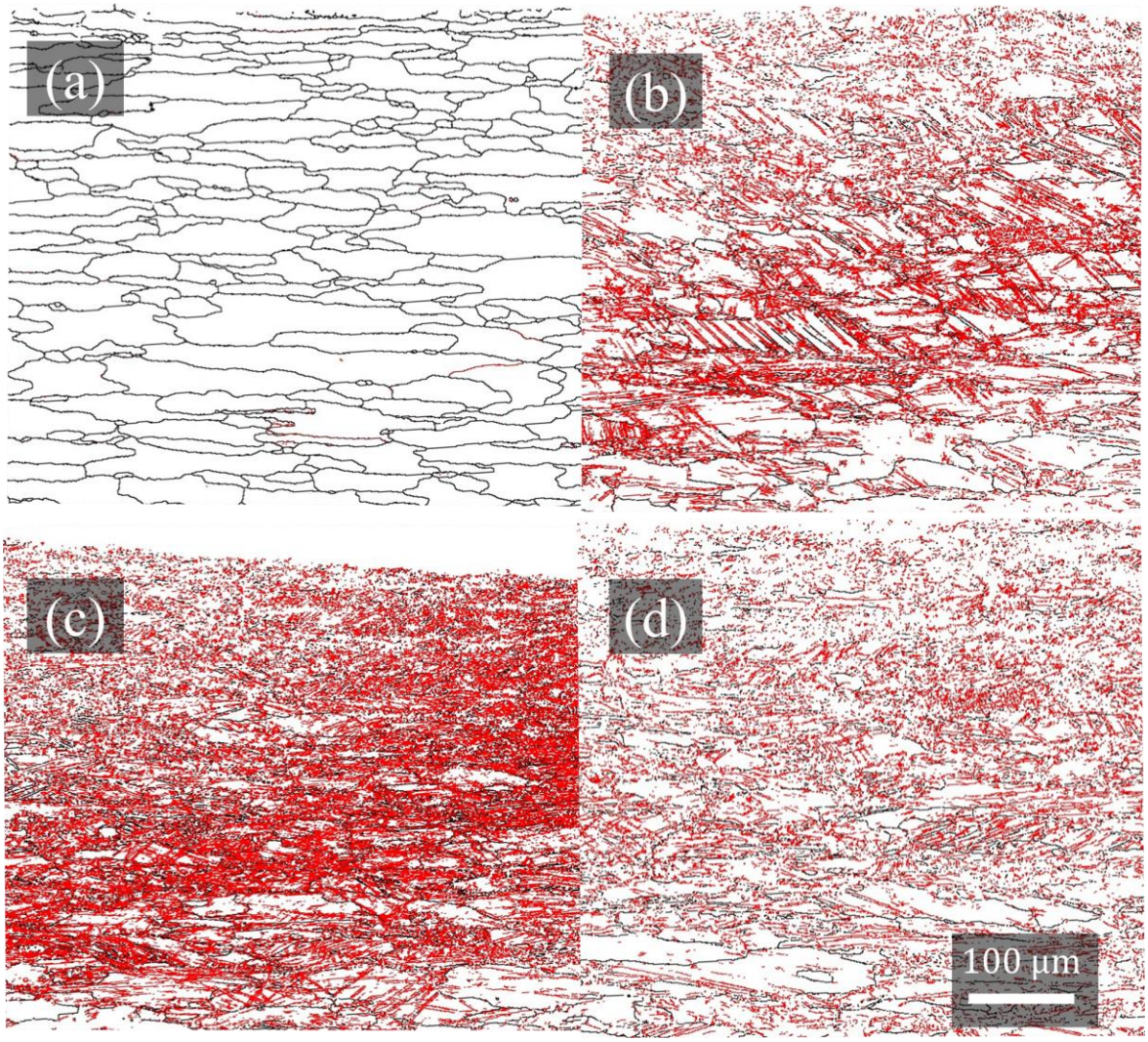

Figure 7. The LAGB and HAGB distribution of (**a**) unMHP, (**b**) MHP1.7, (**c**) MHP2.7, and (**d**) MHP3.5.

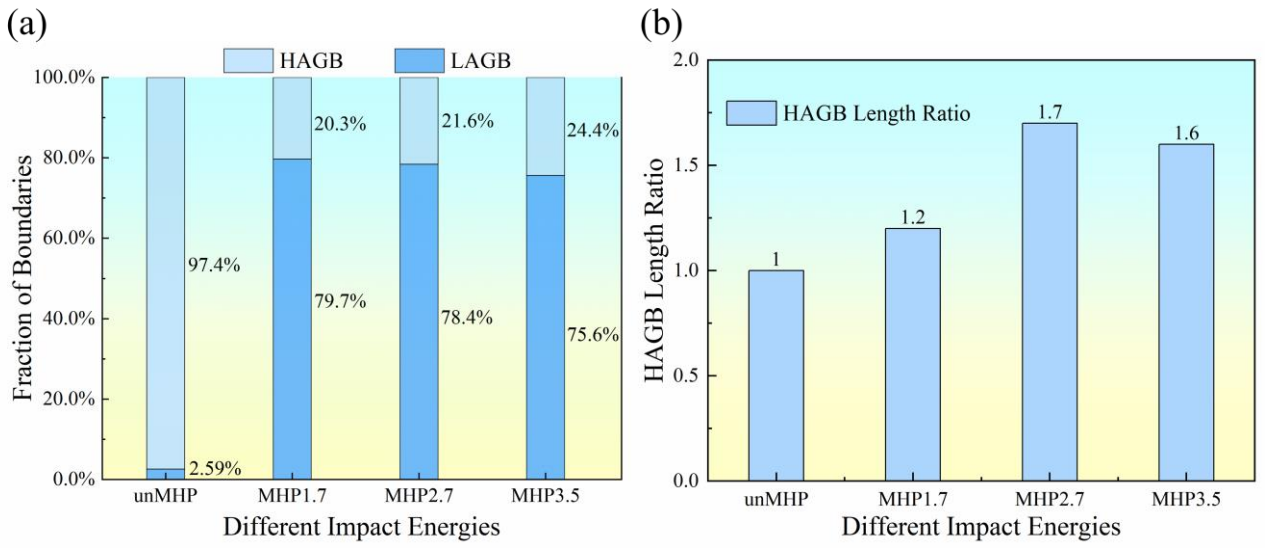

Figure 8. (**a**) The fraction of LAGBs and HAGBs and (**b**) the HAGB length ratio of different MHP samples.

3.3. The Morphology of Impacted Surfaces

Figure 9 displays the surface morphology of A7075 after peening at four distinct energy levels. Figure 9a illustrates the untreated control sample, characterized by a smooth and uniformly colored surface, reflecting the pristine state of the material. The maximum surface height difference of the untreated sample is about 10 μm. Peening induces significant plastic deformation on the Al alloy's surface, creating a rugged surface akin to rolling hills. Theoretically, the size of the depressions correlates directly with the peening head, while their depth is proportional to the energy applied. As the peening energy increases, the degree of plastic deformation intensifies, and the height difference between the highest and lowest surface points also increases. Specifically, when the peening energy rises from 1.7 J to 2.7 J, the surface height difference increases from 121.8 μm to 126.4 μm, accompanied by a reduction in depression diameter. A further increase in energy to 3.5 J results in a significant height difference increase to 200.1 μm, along with a noticeable enlargement of the depression diameter. These changes suggest that higher energy levels lead to deeper plastic deformation.

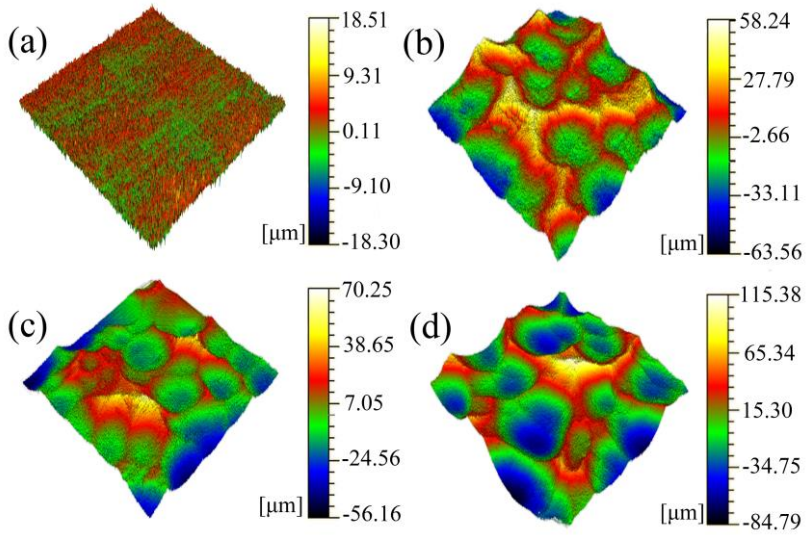

Figure 9. Three-dimensional morphology after MHP treatment: (**a**) unMHP; (**b**) MHP1.7; (**c**) MHP2.7; (**d**) MHP3.5.

It is noteworthy that the depression diameter does not increase linearly with peening energy. At a peening energy of 2.7 J, the sample exhibits the smallest depression size, and the height difference between the surface protrusions and depressions increases by only 4.6 μm compared to 1.7 J. From a morphological perspective, a peening energy of 2.7 J is a more suitable choice as it achieves significant plastic deformation while maintaining relatively low surface roughness. This is further validated in Figure 10, where the sample peened at 2.7 J has the lowest average surface roughness among the peened samples, with Ra values of 3.66 μm and Rt values of 17.51 μm, which is lower than with other surface strengthening methods such as shot peening and cavitation jet usage. For instance, Xu et al. [33], through orthogonal experiments, studied the effect of shot peening on workpiece surface roughness, with the optimal surface roughness in their nine experiments being an Ra value of ~3.79 μm. Liu et al. [34] used cavitation water jet equipment to erode pure copper for different durations, studying the microstructure, damage morphology, surface roughness, and cross-sectional hardness of the samples post-erosion, with surface roughness or Ra values ranging from 3.7 to 9 μm. Additionally, the surface profile line in Figure 10 reveals that compared to the 1.7 J and 3.5 J peened samples, the 2.7 J peened sample has relatively smoother depression edges, a dynamic equilibrium achieved after multiple plastic deformations being the reason for its lower surface roughness. Mechanical hammer peening (MHP) can achieve both surface strengthening and smoothing effects simultaneously; however, the sharp "peak" protrusions on the surfaces of the 1.7 J and 3.5 J peened samples indicate that energy levels that are either too high or too low can lead to surface unevenness. Excessive energy levels can cause over-deformation in localized areas, while insufficient energy levels may fail to act effectively on the material's surface, leading to uneven surface treatment.

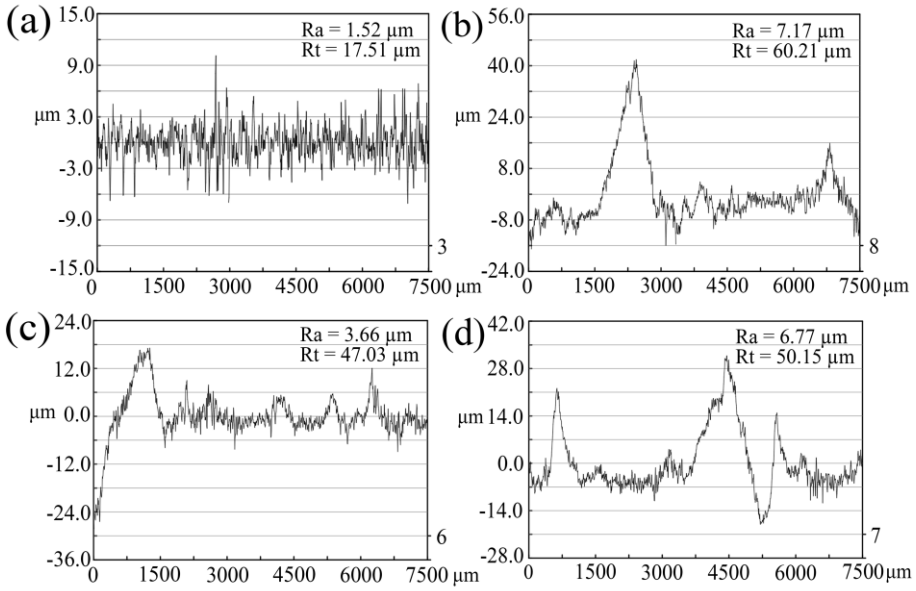

Figure 10. The surface roughness after MHP treatment: (**a**) unMHP; (**b**) MHP1.7; (**c**) MHP2.7; (**d**) MHP3.5.

3.4. Wear Resistance

Figure 11 shows the variation in the friction coefficient of A7075 under a 50 N load, highlighting the frictional behavior and performance of the material during the friction process. In the initial running-in phase, the coefficient of friction increases rapidly as the friction pin disrupts the sample's surface, generating significant heat. This leads to oxidation on the sample's friction surface, with the resulting oxide film providing some lubricative effect. The friction coefficient curve then enters a stable phase, which aligns with the findings reported by Ji-dong Zhang et al. [35]. The figure reveals that the unMHP

sample has a noticeably higher friction coefficient than the hammer-treated samples (MHP1.7, MHP2.7, and MHP3.5), indicating that mechanical hammering strengthens the material. The average friction coefficients for unMHP, MHP1.7, MHP2.7, and MHP3.5 were 0.332, 0.270, 0.272, and 0.274, respectively. Analysis of the results shows that hammer-treated samples have a lower friction coefficient and stronger wear resistance. Additionally, the friction coefficients for the three treated samples are not significantly different during the stable phase, suggesting that mechanical hammering effectively reduces friction and enhances wear resistance, producing a smoother surface. Figure 4 illustrates that the underlying reason for this phenomenon is the introduction of a large number of dislocations, as well as a reduction in grain size, during the hammering process [36]. For A7075 alloy, peening strengthens the material by improving stress distribution, creating a residual compressive stress field, and somewhat suppressing crack formation. These enhancements contribute to increased fatigue life in manufactured components [20].

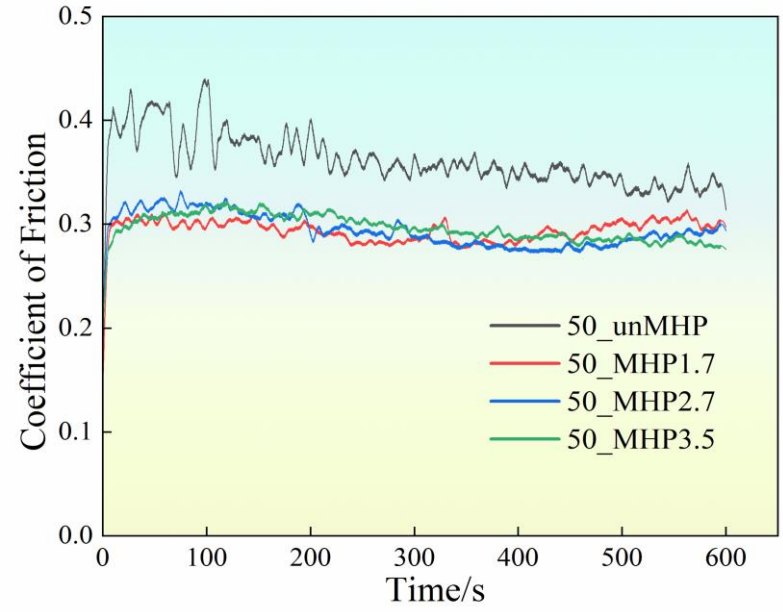

Figure 11. Friction coefficient-time graphs of A7075 after friction and wear under a load of 50 N.

In Figure 12, the wear volume of the material was measured after 600 s of friction and wear under a 50 N load. Wear volume is a critical indicator of wear resistance and is closely linked to the material's service life. Generally, materials with higher hardness exhibit lower wear volumes. The experimental results indicated that the wear volume of hammer-treated samples was significantly lower than that of the untreated samples. Notably, the wear volume of the MHP2.7 sample was only 7.67×10^{-4} mm^3, representing a considerable reduction compared to the untreated samples. Research by Yuting Hao [37] suggests that a lower Ra value can enhance wear resistance, helping explain why the MHP2.7 sample with the lowest Ra value post-treatment exhibits the lowest wear volume. This finding suggests that the hammering treatment can modify the microstructure and surface morphology, resulting in finer surface particles and increased hardness. These changes help prevent abrasive particles from penetrating the material's surface. The plastic deformation induced by hammering promotes the formation of a large number of dislocations, which endows the material with higher strain-hardening ability and greater plastic deformation capacity. According to research by M. Dadgar et al. [36] and the data depicted in Figure 3 and Figure 6, the dislocation generated by mechanical hammering is approximately 400 μm in thickness. Due to the high density of the dislocations, their interaction creates barriers to further dislocation motion, thereby increasing the material's resistance to

deformation. Consequently, samples treated with hammering are less prone to crack formation and crack propagation during repetitive sliding processes.

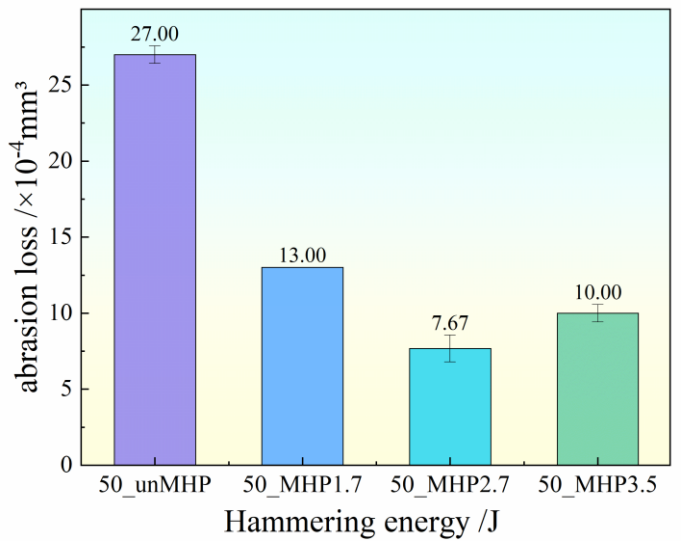

Figure 12. Abrasion loss of A7075 after friction and wear under a load of 50 N.

Figure 13 displays the three-dimensional surface morphology of the unMHP and MHP-7075 samples after friction and wear testing under a 50 N load. Distinct friction and wear grooves are visible on the surface of the unMHP sample, showing typical plowing characteristics due to the material's extrusion along the groove sides during friction. In contrast, the surface of the hammer-treated sample exhibits undulating hammering pits, indicative of work hardening from plastic deformation, which is a key factor in enhancing wear resistance. The increase in hardness results from the combined effects of grain refinement and work hardening [38–41], yielding a higher hardness and improved wear resistance compared to the untreated sample. Unlike the unMHP sample, the hammer-treated sample shows minimal wear marks in the friction and wear test under a 50 N load. In particular, the MHP2.7 sample shows wear grooves with a reddish-yellow color that rise above the average surface height, suggesting that friction and wear have caused only limited damage. Consequently, this sample has the lowest wear volume among all the tested parameters, demonstrating excellent wear resistance.

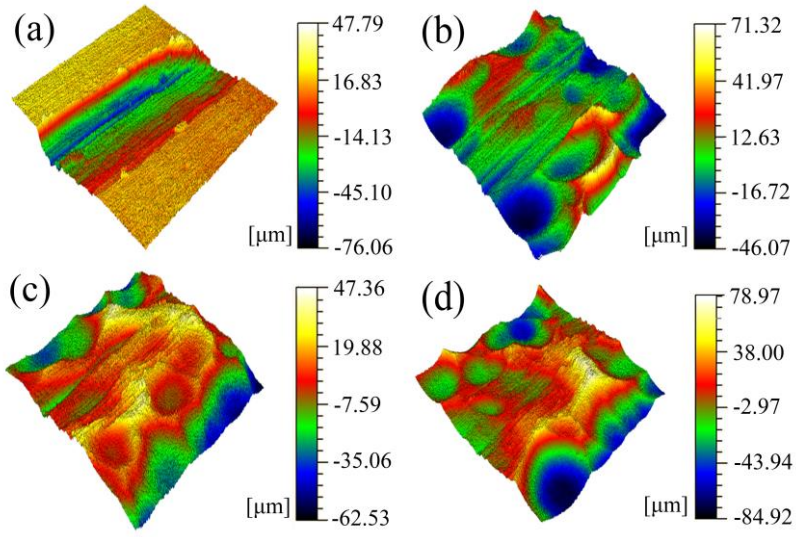

Figure 13. Three-dimensional morphology after treatment: (**a**) unMHP; (**b**) MHP1.7; (**c**) MHP2.7; (**d**) MHP3.5 of wear scars, tested under a load of 50 N.

Figure 14 shows the worn surface morphology of A7075 samples treated with different hammering energies under a 50 N load, as can be observed in the scanning electron microscopy (SEM) images. The low-magnification SEM image in Figure 14a reveals significant oxidation on the surface of the unMHP sample after reciprocating friction and wear, with visible delamination, flaking, and the accumulation of wear debris. These characteristics indicate that the sample experienced oxidative wear along with severe adhesive wear. In the high-magnification SEM image (Figure 14b), delamination is more pronounced, with material flaking off during wear, resulting in an increased surface roughness and further reduction in wear resistance.

The MHP1.7 sample exhibits a relatively smooth friction surface, with only minor scratches and grooves, and minimal surface damage (Figure 14c). High-magnification SEM images reveal some oxides on the surface, indicating that the wear mechanism is primarily mild oxidative wear (Figure 14d). The MHP2.7 sample displays a wave-like layered structure that is approximately perpendicular to the friction direction, which is likely due to the rupture and reformation of the oxide film formed during friction under plastic deformation. This cycle of rupture and reformation leads to the wavy layered pattern visible on the surface (Figure 14e,f). In contrast, the MHP3.5 sample (Figure 14g,h) shows a thicker and more pronounced layering effect than the unMHP, MHP1.7, and MHP2.7 samples, with more visible scratches, possibly indicating mild three-body wear. Comparing the SEM images of the unMHP and hammered samples provides a clear view of the extent of surface damage at a microscopic level due to friction and wear. The hammering treatment significantly enhances the wear resistance of A7075. The MHP1.7 sample demonstrates superior friction resistance compared to MHP2.7 and MHP3.5, suggesting that while hammering improves the surface strength, increasing the hammering energy creates larger surface undulations, which may slightly reduce the friction resistance. Therefore, selecting an optimal hammering energy value is essential for maximizing the material's wear resistance.

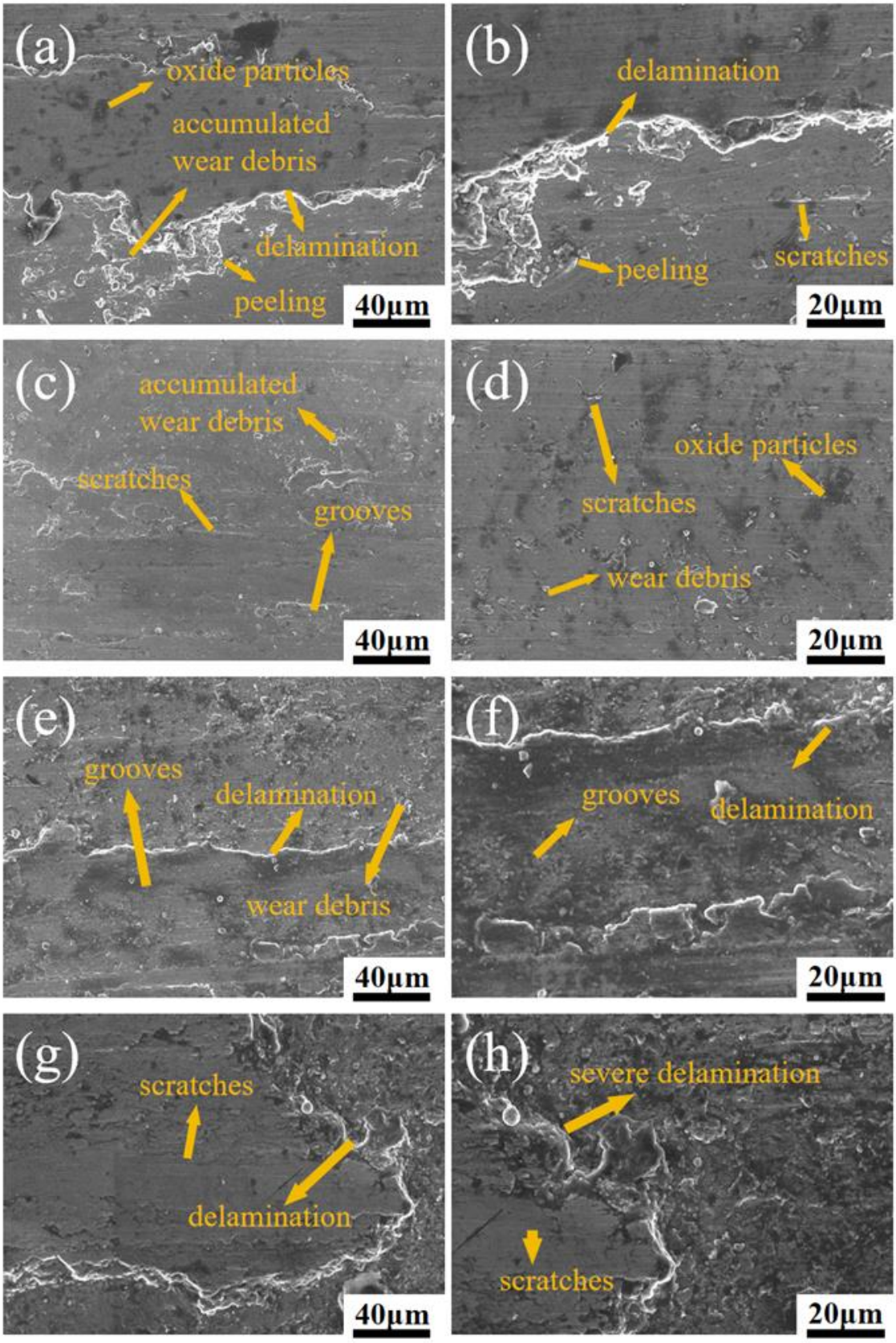

Figure 14. SEM images of: (**a**,**b**) unMHP; (**c**,**d**) MHP1.7; (**e**,**f**) MHP2.7; (**g**,**h**) MHP3.5, showing the wear scars when tested under a load of 50 N.

Following the tribological testing of A7075 alloy under a load of 50 N, energy-dispersive spectroscopy (EDS) analysis was conducted on a specific area within the MHP2.7 region that encompasses the tribological wear boundary. The results of this analysis are presented in Figure 15, where the orange dashed line delineates the boundary of tribological wear. It is evident from the figure that there is a significant disparity in the concentration of oxygen elements on either side of the wear boundary, which serves as direct evidence for the ubiquity of oxidative wear during the tribological process. Based on the elemental distribution from the EDS mapping analysis, Al_2O_3 was identified as the dominant oxidation product in the worn region, which corresponds to the high Al content in the matrix material. Additionally, a small amount of MgO was detected in the oxide layer.

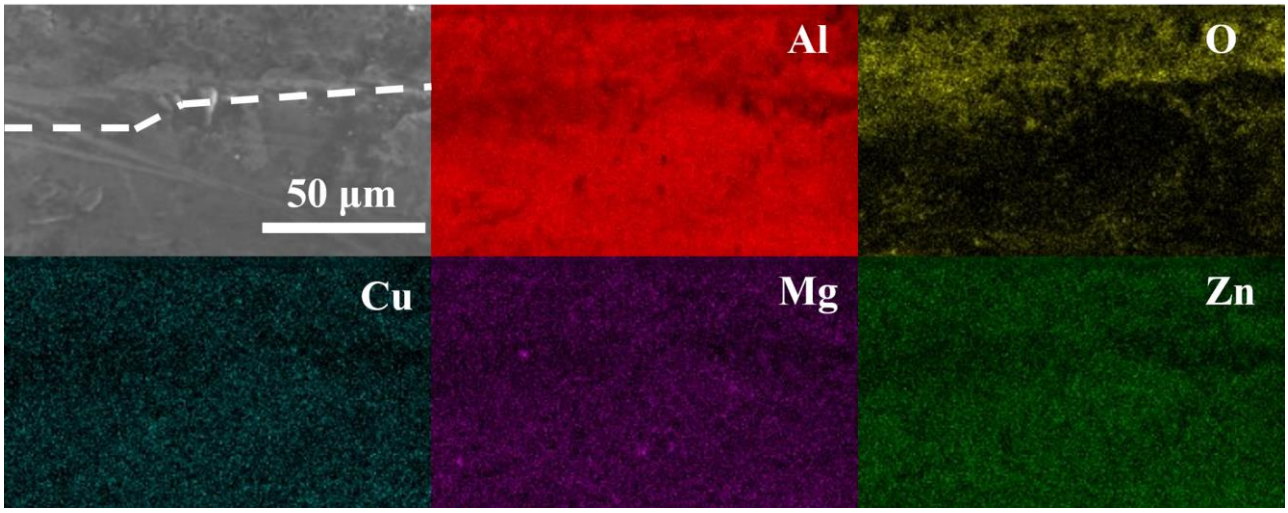

Figure 15. EDS images of MHP2.7.

4. Conclusions

The enhancement of 7075 aluminum alloy (A7075) through MHP treatment was investigated, focusing on the material's microhardness, surface morphology, and tribological properties under various peening energy levels. The conclusions are as follows:

1. After MHP, the surface and sub-surface hardness of A7075 were significantly increased, with the peening energy capable of reinforcing to a depth of 2 mm. Compared to the untreated samples, the microhardness of the sample treated with a peening energy of 3.5 J (MHP3.5) increased by approximately 21%, indicating that MHP effectively improves the surface hardness of A7075.
2. MHP treatment induces grain refinement and increases the density of GNDs in A7075, especially in the near-surface region. At an impact energy of 2.7 J, the grain size reached its minimum, and GND density was highest, indicating optimal strengthening.
3. The surface of A7075 without MHP was smooth and uniform. After peening treatment, the surface exhibited a mountainous pattern of pits, with the pit diameter and surface roughness first decreasing and then increasing with the increase in peening energy, indicating that 2.7 J is the optimal peening energy for roughness.
4. MHP significantly enhanced the wear resistance of A7075. Compared to the control group, the peened samples exhibited lower coefficients of friction and wear volume, with the sample peened at 2.7 J (MHP2.7) having a wear volume of 7.67×10^{-4} mm^3. Under a load of 50N, the wear traces on the surface of the peened samples were not apparent, especially in the case of the MHP2.7 sample, where the wear groove was above the average height and the damage to the surface from friction and wear was extremely limited.

5. Under a load of 50N, the untreated sample (unMHP) exhibited oxidative wear and severe adhesive wear. In contrast, the sample with an impact energy of 1.7 J (MHP1.7) had a relatively smooth friction surface with only a few scratches and pits, indicating minor surface damage. After MHP treatment, the wear mechanisms of A7075 primarily consisted of oxidative wear and three-body wear. MHP has a significant strengthening effect on the wear resistance of A7075, and selecting the appropriate reinforcement energy is crucial for enhancing the wear resistance of the material.

Author Contributions: Conceptualization, Y.L. and Y.W.; methodology, L.Y. and Y.Y.; software, Y.L. and L.Y.; validation, Y.W., L.Y., and N.N.; formal analysis, X.W. and Y.S.; investigation, X.W. and Y.S.; resources, Y.Y. and N.N.; data curation, Y.Y. and Y.S.; writing—original draft preparation, L.Y., Y.L., and X.W.; writing—review and editing, Y.W., N.N., and Y.Y.; visualization, Y.W., Y.L., and N.N.; supervision, X.W. and Y.S. All authors have read and agreed to the published version of the manuscript.

Funding: The research was supported by the Priority Academic Program Development of Jiangsu Higher Education Institutions (PAPD), Jiangsu Innovation Support Program (International Science and Technology Cooperation) Project (grant number BZ2023002), the Large Instruments Open Foundation of Nantong University (KFJN2428), the Analysis and Test Centre of Nantong University, and the Analysis and Testing Center of NUAA.

Institutional Review Board Statement: Not applicable.

Informed Consent Statement: Not applicable.

Data Availability Statement: Data is contained within the article.

Conflicts of Interest: No conflict of interest exists in the submission of this manuscript, and the manuscript was approved by all authors for publication.

References

1. Sun, Q.; Han, Q.; Wang, S.; Xu, R. Microstructure, corrosion behaviour and thermal stability of AA 7150 after ultrasonic shot peening. *Surf. Coat. Technol.* **2020**, *398*, 126127. https://doi.org/10.1016/j.surfcoat.2020.126127.
2. Yang, W.; Ji, S.; Zhang, Q.; Wang, M. Investigation of mechanical and corrosion properties of an Al–Zn–Mg–Cu alloy under various ageing conditions and interface analysis of η′ precipitate. *Mater. Des.* **2015**, *85*, 752–761. https://doi.org/10.1016/j.matdes.2015.06.183.
3. Chen, S.; Chen, K.; Peng, G.; Jia, L.; Dong, P. Effect of heat treatment on strength, exfoliation corrosion and electrochemical behavior of 7085 aluminum alloy. *Mater. Des.* **2012**, *35*, 93–98. https://doi.org/10.1016/j.matdes.2011.09.033.
4. Kumar, P.; Mahobia, G.; Mandal, S.; Singh, V.; Chattopadhyay, K. Enhanced corrosion resistance of the surface modified Ti-13Nb-13Zr alloy by ultrasonic shot peening. *Corros. Sci.* **2021**, *189*, 109597.
5. Wang, H.; Ning, C.; Huang, Y.; Cao, Z.; Chen, X.; Zhang, W. Improvement of abrasion resistance in artificial seawater and corrosion resistance in NaCl solution of 7075 aluminum alloy processed by laser shock peening. *Opt. Lasers Eng.* **2017**, *90*, 179–185.
6. Amini, S.; Kariman, S.A.; Teimouri, R. The effects of ultrasonic peening on chemical corrosion behavior of aluminum 7075. *Int. J. Adv. Manuf. Technol.* **2017**, *91*, 1091–1102. https://doi.org/10.1007/s00170-016-9795-6.
7. Abeens, M.; Muruganandhan, R.; Thirumavalavan, K. Comparative Analysis of Different Surface Modification Processes on AA 7075 T651. *IOP Conf. Ser. Mater. Sci. Eng.* **2019**, *574*, 012018. https://doi.org/10.1088/1757-899X/574/1/012018.
8. Tan, C.Y.; Wen, C.; Ang, H.Q. Influence of laser parameters on the microstructures and surface properties in laser surface modification of biomedical magnesium alloys. *J. Magnes. Alloys* **2024**, *12*, 72–97. https://doi.org/10.1016/j.jma.2023.12.008.
9. Liao, L.; Gao, R.; Yang, Z.H.; Wu, S.T.; Wan, Q. A study on the wear and corrosion resistance of high-entropy alloy treated with laser shock peening and PVD coating. *Surf. Coat. Technol.* **2022**, *437*, 128281. https://doi.org/10.1016/j.surfcoat.2022.128281.
10. Dong, J.; Wu, H.; Chen, Y.; Zhang, Y.; Wu, Y.; Yin, S.; Du, Y.; Hua, K.; Wang, H. Study on self-lubricating properties of AlCoCrFeNi2.1 eutectic high entropy alloy with electrochemical boronizing. *Surf. Coat. Technol.* **2022**, *433*, 128082. https://doi.org/10.1016/j.surfcoat.2022.128082.
11. Luo, H.; Long, B.; Lu, S.; Guo, L.; Luo, F.; Lin, W.; Cao, J.; Yin, Z.; Zhao, P. Dislocation loops, segregation and hardening induced by high-dose ion irradiation of NbMoTaW and VCrTaW high-entropy alloy coatings on the T91 substrate. *Surf. Coat. Technol.* **2023**, *473*, 130019. https://doi.org/10.1016/j.surfcoat.2023.130019.
12. Huang, T.-C.; Hsu, S.-Y.; Lai, Y.-T.; Tsai, S.-Y.; Duh, J.-G. Effect of NiTi metallic layer thickness on scratch resistance and wear behavior of high entropy alloy (CrAlNbSiV) nitride coating. *Surf. Coat. Technol.* **2021**, *425*, 127713. https://doi.org/10.1016/j.surfcoat.2021.127713.
13. Yang, H.; Tang, Z.; Wan, L.; Wei, Q.; Wu, J.; Wang, A.; Jin, X.; Li, X.; Wu, Y.; Lu, G.; et al. Achieving crack-free CuCrZr/AlSi7Mg interface by infrared-blue hybrid laser cladding with low power infrared laser. *J. Alloys Compd.* **2023**, *931*, 167572. https://doi.org/10.1016/j.jallcom.2022.167572.

14. Lian, Q.; Deng, G.; Al-Juboori, A.; Li, H.; Liu, Z.; Wang, X.; Zhu, H. Crack propagation behavior in white etching layer on rail steel surface. *Eng. Fail. Anal.* **2019**, *104*, 816–829. https://doi.org/10.1016/j.engfailanal.2019.06.067.
15. Li, J.; Chen, J.; Huang, Q.; Wu, L.; Cao, F.; Sun, Q. Effect of surface contamination on electrochemical corrosion behavior of ultrasonic shot peened TA2 alloy. *J. Mater. Res. Technol.* **2024**, *29*, 3575–3584. https://doi.org/10.1016/j.jmrt.2024.02.114.
16. Zhang, Z.; Yang, Y.; Gao, Y.; Wang, G.; Shi, W. Performance Analysis of 7075 Aluminum Alloy Strengthened by Cavitation Water Jet Peening at Different Scanning Speeds. *Crystals* **2022**, *12*, 1451. https://doi.org/10.3390/cryst12101451.
17. Sundar, R.; Ganesh, P.; Gupta, R.K.; Ragvendra, G.; Pant, B.K.; Kain, V.; Ranganathan, K.; Kaul, R.; Bindra, K.S. Laser Shock Peening and its Applications: A Review. *Lasers Manuf. Mater. Process.* **2019**, *6*, 424–463. https://doi.org/10.1007/s40516-019-00098-8.
18. Tao, Y.; Ma, Q.; Lu, Y.; Huang, D.; Zhang, H. Improvement of thermal shock resistance and hot mechanical properties by FCC/BCC/B2 multiphase strengthened microstructure in laser cladded high-entropy alloy coatings. *Surf. Coat. Technol.* **2023**, *472*, 129919. https://doi.org/10.1016/j.surfcoat.2023.129919.
19. Liu, Q.; Jin, S.; Shen, B. Precisely tuning the residual stress anisotropy in machine hammer peening. *Int. J. Adv. Manuf. Technol.* **2023**, *127*, 4577–4589. https://doi.org/10.1007/s00170-023-11828-w.
20. Liu, Q.; Chen, S.; Xu, X.; Jin, S.; Li, Y.; Wang, Y.; Shen, B. Multi-objective optimization of the subsurface residual stress field of TC4 alloy in machine hammer peening. *J. Manuf. Process.* **2023**, *104*, 98–107. https://doi.org/10.1016/j.jmapro.2023.09.002.
21. Lin, X.H.; Huang, H.B.; Zhou, C.S.; Liu, J.C.; Saleh, M.; Wang, Z.Z. Research on surface modification of anodized aluminum alloy using piezoelectric machine hammer peening. *Int. J. Adv. Manuf. Technol.* **2019**, *104*, 1211–1219. https://doi.org/10.1007/s00170-019-04016-2.
22. Jin, S.; Liu, Q.; Zhu, Y.; Shen, B. Surface smoothening and strengthening combined effect of mechanical hammer peening on inconel 718 superalloy. *Mater. Manuf. Process.* **2023**, *38*, 1331–1337. https://doi.org/10.1080/10426914.2022.2146722.
23. Klotz, T.; Delbergue, D.; Bocher, P.; Lévesque, M.; Brochu, M. Surface characteristics and fatigue behavior of shot peened Inconel 718. *Int. J. Fatigue* **2018**, *110*, 10–21.
24. Kattoura, M.; Telang, A.; Mannava, S.R.; Qian, D.; Vasudevan, V.K. Effect of Ultrasonic Nanocrystal Surface Modification on residual stress, microstructure and fatigue behavior of ATI 718Plus alloy. *Mater. Sci. Eng. A* **2018**, *711*, 364–377.
25. Kumar, D.; Idapalapati, S.; Wang, W.; Child, D.J.; Haubold, T.; Wong, C.C. Microstructure-mechanical property correlation in shot peened and vibro-peened Ni-based superalloy. *J. Mater. Process. Technol.* **2019**, *267*, 215–229.
26. Dadgar, M.; Gräfe, S.; Müller, M.; Herrig, T.; Bergs, T. Influences of Machine Hammer Peening on Inconel 718 Workpieces Manufactured by Wire-based Laser Metal Deposition. *Procedia CIRP* **2024**, *121*, 192–197. https://doi.org/10.1016/j.procir.2023.08.064.
27. Bleicher, F.; Lechner, C.; Habersohn, C.; Obermair, M.; Heindl, F.; Rodriguez Ripoll, M. Improving the tribological characteristics of tool and mould surfaces by machine hammer peening. *CIRP Ann.* **2013**, *62*, 239–242. https://doi.org/10.1016/j.cirp.2013.03.043.
28. Rodríguez Ripoll, M.; Heindl, F.; Lechner, C.; Totolin, V.; Jech, M.; Bleicher, F. Enhanced Sliding Wear Resistance of Technical Alloys by Hard Particle Reinforcement Using Machine Hammer Peening. *Tribol. Trans.* **2017**, *60*, 479–789. https://doi.org/10.1080/10402004.2016.1178828.
29. Kuczyk, M.; Kotte, L.; Kaspar, J.; Zimmermann, M.; Leyens, C. Alloy Design and Microstructure Evolution in the AlxCoCrFeNi Alloy System Synthesized by Laser Metal Deposition. *Front. Mater.* **2020**, *7*, 242. https://doi.org/10.3389/fmats.2020.00242.
30. Mostafa, A.M.; Hameed, M.F.; Obayya, S.S. Effect of laser shock peening on the hardness of AL-7075 alloy. *J. King Saud Univ.-Sci.* **2019**, *31*, 472–478. https://doi.org/10.1016/j.jksus.2017.07.012.
31. Qiao, X.G.; Starink, M.J.; Gao, N. Hardness inhomogeneity and local strengthening mechanisms of an Al1050 aluminium alloy after one pass of equal channel angular pressing. *Mater. Sci. Eng. A* **2009**, *513–514*, 52–58. https://doi.org/10.1016/j.msea.2009.01.051.
32. Zhang, J.; Gao, N.; Starink, M.J. Microstructure development and hardening during high pressure torsion of commercially pure aluminium: Strain reversal experiments and a dislocation based model. *Mater. Sci. Eng. A* **2011**, *528*, 2581–2591. https://doi.org/10.1016/j.msea.2010.11.079.
33. Wujiao, X.; Chengshang, L.; Xinyao, L. Simulation and prediction of surface roughness of 6061 aluminum alloy workpiece after shot peening. *J. Jilin Univ. (Eng. Technol. Ed.)* **2019**, *49*, 1280–1287.
34. Liu, H. Cavitation Damage on Surface of Pure Copper by Cavitating Water Jet Erosion. *Mater. Mech. Eng.* **2017**, *41*, 68–73.
35. Zhang, J.-D.; Zhang, L.; Ma, H.-Z. Effect of ZrO_2 additions on the microstructure, mechanical and wear properties of ZrO2/7075 aluminium alloy composite. *Mater. Today Commun.* **2023**, *37*, 107437. https://doi.org/10.1016/j.mtcomm.2023.107437.
36. Dadgar, M.; Gräfe, S.; Müller, M.; Herrig, T.; Bergs, T. Surface Integrity of Additively Manufactured Workpieces after Machine Hammer Peening. *Procedia CIRP* **2024**, *123*, 161–166. https://doi.org/10.1016/j.procir.2024.05.030.
37. Hao, Y.; Ye, Z.; Ye, M.; Dong, H.; Wang, L.; Du, Y. Construction and growth of black PEO coatings on aluminum alloys for enhanced wear and impact resistance. *Ceram. Int.* **2023**, *49*, 30782–30793. https://doi.org/10.1016/j.ceramint.2023.07.034.
38. Liu, H.; Wei, Y.; Tan, C.K.I.; Ardi, D.T.; Tan, D.C.; Lee, C.J. XRD and EBSD studies of severe shot peening induced martensite transformation and grain refinements in austenitic stainless steel. *Mater. Charact.* **2020**, *168*, 110574.
39. Chen, L.; Ren, X.; Zhou, W.; Tong, Z.; Adu-Gyamfi, S.; Ye, Y.; Ren, Y. Evolution of microstructure and grain refinement mechanism of pure nickel induced by laser shock peening. *Mater. Sci. Eng. A* **2018**, *728*, 20–29.

40. Hönnige, J.; Davis, A.E.; Ho, A.; Kennedy, J.R.; Neto, L.; Prangnell, P.; Williams, S. The effectiveness of grain refinement by machine hammer peening in high deposition rate wire-arc AM Ti-6Al-4V. *Metall. Mater. Trans. A* **2020**, *51*, 3692–3703.
41. Yin, F.; Zhang, X.; Chen, F.; Hu, S.; Ming, K.; Zhao, J.; Xie, L.; Liu, Y.; Hua, L.; Wang, J. Understanding the microstructure refinement and mechanical strengthening of dual-phase high entropy alloy during ultrasonic shot peening. *Mater. Des.* **2023**, *227*, 111771.